0

Plasma Enhanced Chemical Vapor Deposition Of Thin Films From Organosilicon Compounds

Lenka Zajíčková and Vilma Buršíková
Masaryk University
Czech Republic

1. Introduction

Compounds of an organosilicon group provide a large variety of possible reactants for either chemical vapor deposition (CVD) or plasma enhanced CVD (PECVD) processes. They are generally sufficiently volatile near the room temperature, relatively non-toxic and non-flammable, cheap and available from commercial resources Wrobel & Wertheimer (1990). Due to their organic-inorganic character they can be used for deposition of polymers as well as inorganic coatings. Silicon oxide films, for example, can be prepared by PECVD when organosilicon vapors are mixed with oxygen Pai & Chang (1990); Ray et al. (1992); Ebihara et al. (1993). It should be stressed that the character of deposited materials can be gradually changed from organic to inorganic chemical structure simply by the variation of processes parameters Vallée et al. (2000). Therefore, PECVD films from organosilicon compounds overcomes the limitations of conventional organic or inorganic materials and their research contributes to the development of so called hybrid materials that exhibit unique or enhanced properties compared to the their single organic or inorganic competitors.

Hybrid organic-inorganic materials, that were developed in the past 20 years, can be classified into two major classes according to the kind of molecular bonds/interactions **?**. The class I comprises materials exhibiting interactions like van der Waals forces or hydrogen bonds between organic and inorganic parts. These materials form micro or nanocomposites in which one part (organic or inorganic) is dispersed in the other one acting as the host matrix. The class II consists of materials with covalent bonding between organic and inorganic parts, resulting usually in a homogeneous hybrid material at the molecular level.

Materials of the class I prepared by pure chemical methods include nanosized silica particles in a polymer matrix for potential applications in optical devices **??** or microporous silica beads in a polymer matrix for gas separation **?**. Chemically synthesized heteropoly-siloxanes, i.e. hybrid materials of the class II, exhibited selective transport properties and were suggested, therefore, as membranes or active parts of chemical sensors **?**.

Organosilicon compounds, such as e.g. tetraethoxysiloxane ($C_8H_{20}O_4Si$ - TEOS), hexamethyldisiloxane ($C_6H_{18}OSi_2$ - HMDSO) and octamethylcyclotetrasiloxane ($C_8H_{24}O_4Si_4$ - OMCTS), are suitable for the chemical synthesis of hybrid materials of both classes [6] and are also employed for PECVD. The latter method combines physical and chemical processes in the plasma phase as well as at plasma-solid interface. It is based on the molecule dissociation in the gas phase by impact of energetic electrons and atoms in metastable states followed by chemical reactions of gas radicals.

As compared with classical chemical methods, PECVD has several advantages: low substrate temperature (necessary condition in many applications), possibility to produce materials of new properties and to vary the film properties simply by changing some deposition parameters, film production without toxic by-products, ozone and the like. It hase already established a key role in many industrial products such as microelectronic devices, solar cells, protective or anticorrosion coatings on machining tools or automobile parts. In many other cases, it is still an emerging technology with a large potential for further grow. However, there is always a need for better understanding of plasmachemical processes and testing different deposition conditions as well as new mixtures and multi-step procedures **?**.
PECVD of silicon oxide films from TEOS monomer has been studied since 60ties when Alt *et al.*Alt et al. (1963), Ing *et al.*Ing & Jr. (1965) and Secrist *et al.*Secrist & Mackenzie (1966) published results of a new deposition method based on a glow discharge in $TEOS/O_2$ vapours. Hexamethyldisiloxane ($C_6H_{18}OSi_2$ - HMDSO) is often preferred in the case of plasma polymerization because of its higher organic character as well as high vapor pressure. The plasma polymerization in HMDSO/Ar mixtures has been tested already in 70-ties Tien et al. (1972); Vasile & Smolinski (1972).

2. Applications of Silicon Oxide Thin Films

The fabrication of electronic components, especially microelectronic integrated circuits, have undoubtedly found the widest and most demanding application for thin film depositions Rossnagel et al. (1989). An important aspect of microelectronics technology involves the deposition of dielectric thin films such as silicon dioxide (SiO_2). These films are mainly used as an insulating layer between interconnect levels or passivation layer over devices Chin & de Ven (1988); Selamoglu et al. (1989); Pai & Chang (1990). They have to exhibit good electrical properties, low stress and created void-free, conformal fillings over fine features, i. e., good step coverage. In very large scale integrated (VLSI) circuit technology the deposition of interlevel dielectrics requires a low temperature process ($< 400\ ^\circ C$) since the first level metal (normally aluminum) is already deposited and any subsequent high temperature processing may destroy the devices. In advanced ultra-large scale integration (ULSI) the current trends are characterized by yet lower process temperature and requirements of better step coverage on high aspect ratio features. Therefore, PECVD of SiO_2 is preffered over the thermal CVD method.
Silicon oxides were tested for metal protection against corrosion and for pigments protection against photodegradation **?**. Low temperature silicon oxide is a suitable material for transparent hard coatings on plastics, e. g., polymethylmethacrylate or polycarbonate Kageyama & Taga (1987); Reed et al. (1989); Bauser et al. (1994). SiO_2 thin films were used for antireflection coatings and thermal stabilization of solar cells **??** as well as for improving the moisture and the gas barrier capability of membranes Levy et al. (1996), Williams et al. (1994).

3. Applications of Organosilicon Plasma Polymers

The above applications do not always require SiO_2-like films. Polymers with appreciable organic fraction, deposited from organosilicon compounds without oxygen addition, are usually suitable for many of them. The presence of an organic fraction in the film matrix could even improve the adhesion to plastics, decrease the stress and lead to more stable films acting often as an intermediate layer between a plastic substrate and a hard anorganic silicon oxide film D. Korzec & Engemann (1996); Reed et al. (1991). An optical clarity, low absorption,

low scattering losses, an ability to "tailor" refractive index and to prepare scratch-resistant films render plasma polymerized (PP) organosilicon films attractive for optical applications. They were also found to provide good corrosion protection to Al coatings and other metals Schreiber et al. (1980); **?**); Angelini et al. (2002). Protective overcoats of PP-HMDSO on evaporated Al in automobile headlight reflectors probably represent the largest single industrial application of plasma polymer films. The PP organosilicon films can be used as barrier films for food and pharmaceutical packaging, coatings for biocompatible materials and low-k dielectric layers for microelectronic applications Borvon et al. (2002; 2003). At the moment a great deal of applicative work can be found in the field of protective anti-scratch coatings on plastic substrates, especially polycarbonates Wydeven (1977); Hollahan & T. Wydeven (1977); Benz et al. (1985); D. Korzec & Engemann (1996); Zajíčková et al. (1998; 2001); Zajíčková, Buršíková, Kučerová, Franta, Dvořák, Šmíd, Peřina & Macková (2007).

4. Deposition in low pressure radio frequency capacitive discharges

The present paper compares properties of thin films deposited from two different organosilicons, hexamethyldisiloxane (HMDSO) and octamethylcyclotetrasiloxane (D4), in radio frequency (rf) capacitive discharges (13.56 MHz). The reactor chamber consisted of a stainless steel cylinder, 490 mm in inner diameter and 246 mm in height, closed by two stainless steel flanges. The substrates were placed on the rf bottom electrode, 20 mm in thickness and 420 mm in diameter. The detail drawing of the reactor is in Fig. **??**.
Due to an asymmetric capacitive coupling and different mobility of electrons and ions a negative dc self-bias U_{bias} was superimposed over the rf voltage. Therefore, positive ions were accelerated toward the substrates and the self-bias affected the ion bombardment of the growing film. At low pressure the energy of ions was approximately equal to $|U_{\mathrm{b}}|$.

5. Methods for characterization of film structure and properties

The chemical structure of the films was studied by FTIR. Their atomic composition was determined by a combination of Rutherford backscattering spectroscopy (RBS) and elastic recoil detection analysis (ERDA).
The Fischerscope H100 depth sensing indentation (DSI) tester equipped with Vickers indenter was used to study the mechanical properties of the coating-substrate systems. In the case of this tester the applied load is registered as a function of indentation depth both during loading and unloading period. The indentation tests were performed in the range from 2 to 200 mN. In order to obtain proper description of the indentation response for the whole system at least 10 different maximum loads were chosen. Each indentation test was repeated at least 16 times in order to minimize the experimental error. The indentation depth was determined with precision of ± 1 nm. From the loading-unloading curves it is possible to obtain the Martens hardness HM (also so called universal hardness), the total deformation work W_{tot}, the elastic deformation work W_{e} and the irreversible dissipated indentation work W_{irr}. The Martens hardness HM is the measure of the resistance against elastic and plastic deformation:

$$HM = \frac{L}{A(h)} = \frac{L}{26.43h^2} \tag{1}$$

where $A(h)$ is the contact area between the indentor and tested material, h is the penetration depth (corrected to the real indentor shape) for the given applied load L and 26.43 is a factor characterizing the Vickers indenter geometry. The total deformation work W_{tot}, the elastic

deformation work W_e and the irreversible dissipated indentation work W_{irr} can be expressed as follows :

$$W_{tot} = \int_{h_0}^{h_{max}} L_1(h)dh, \qquad W_e = \int_{h'_r}^{h_{max}} L_2(h)dh, \qquad W_{irr} = W_{tot} - W_e \tag{2}$$

where $L_1(h)$ and $L_2(h)$ are the loading and unloading curves, respectively and h_{min} and h_{max} denote the penetration depths at the minimum and maximum loads, respectively and h'_r is reduced penetration depth. From the load-penetration curves it is possible to determine also the material resistance against plastic deformation H_{pl} (so called plastic hardness) or H_{IT} (so called indentation hardness) and the indentation elastic modulus E_{IT}.

$$H_{pl} = \frac{L_{max}}{A_t}, \qquad H_{IT} = \frac{L_{max}}{A_p} \tag{3}$$

where A_t is the area of the remained indentation print created by irreversible deformation under maximum load L_{max}, A_p is the projection of the indentation print area (projected contact area). The A_t to A_p ratio is 1.0785 in case of four-sided pyramid indenter Vickers and its value is 1.1030 in case of three-sided Berkovich pyramid indenter.
The unloading part of the load-penetration curve is usually used to determine the contact stiffness S, the remained contact depth h_f and the reduced elastic modulus E_r. The unloading stiffness is determined as the slope of the tangent to the unloading data at maximum load.

$$h_f = h_{max} - \varepsilon\frac{L_{max}}{S}, \qquad S = \frac{dL}{dh} \tag{4}$$

Here ε=1 for a cylindrical punch approximation while ε=0.75 is used for Vickers or Berkovich indenters to eliminate the sinking-in effect. The indentation elastic modulus E_{IT} of the tested material can be calculated on the basis of the contact model **?** in the following way:

$$\frac{1}{E_{IT}} = \frac{1-\nu^2}{E} = \frac{1}{E_r} - \frac{1-\nu_i^2}{E_i}, \qquad E_r = \frac{\sqrt{\pi}S}{2\sqrt{A_p}} \tag{5}$$

Here E, E_i, ν and ν_i are the Young's modulus of either film or the diamond indentor and the Poisson's ratio of either film or the diamond indentor, respectively.
The contact model was derived on the basis of the homogeneous elastic half space assumption, which is not fulfilled for thin films on substrates with different elastic properties. Therefore, it is necessary to measure the film in depths, where the substrate influence is negligible, otherwise the calculated value of the indentation elastic modulus E_{IT} represents an average of elastic constants of the coating and the substrate for the given indentation depth. This statement holds also for both indentation and plastic hardness.
Very useful value used to test the indentation response of nonhomogeneous materials is the so called differential hardness DH

$$DH = \frac{\partial L}{k\partial h^2}, \tag{6}$$

where k is the geometrical factor characterising the indentor shape. The differential hardness, DH, gives information about the strain response of the material to a small change in indentation load and it is used to visualizee the possible changes in the material (differences in surface and bulk properties, heterogeneities, creation of defects, increasing influence of the substrate).

From the dependence of DH on the indentation depth it is possible to determine the indentation depth with minimum substrate influence. This dependence enables also to visualise the crack creation, what appears on the depth dependence of DH as an abrupt jump.

6. Deposition from 5 % HMDSO/O_2 gas feed at pressure 40 and 2.5 Pa

As mentioned above inorganic silicon oxide films can be prepared from organosilicon compounds highly diluted in oxidant gases such as oxygen, ozone, CO etc. Ray et al. (1992), Kulisch et al. (1989), Fujino et al. (1992).

High dilution of the monomer is not the only precondition for preparation of good quality silicon dioxides. It has been shown for the deposition in capacitively coupled radio frequency plasma of HMDSO/O_2 that other external parameters influenced significantly composition and properties of these films Zajíčková, Buršíková, Franta, Bousquet, Granier, Goullet & Buršík (2007); Zajíčková, Buršíková, Kučerová, Franta, Dvořák, Šmíd, Peřina & Macková (2007). Two depositions from 5 % of HMDSO diluted in oxygen were carried out at the same rf power, 100 W, and different pressures, 40 and 2.5 Pa. The lower pressure was achieved by decreased total flow rate from 84 to 15 sccm. The changed conditions corresponded also to different gas residence time, 12 and 4 s, respectively. Since dc self-bias U_b is in a relation with the rf power as well as the pressure Zajíčková, Buršíková, Kučerová, Franta, Dvořák, Šmíd, Peřina & Macková (2007) its magnitude differed for different pressure as shown in Table 3. The energy of ions bombarding the growing film was much lower in case of higher pressure as a consequence of lower self-bias and increased probability of collisions in the sheath adjacent to the substrate.

Differences in the chemical structure of the films deposited from 5 % HMDSO/O_2 at different pressures can be seen by comparison of their absorbances in IR region (Figs. 1 and 2). The overview spectra in Fig. 1 are dominated by three characteristic peaks of silica at 440–450, 800–806 and 1059–1076 cm^{-1} corresponding to the rocking, bending and stretching vibrations of the Si-O-Si groups, respectively **?**. Additional observed absorption peaks corresponded to the impurities such as hydrogen and carbon. As discussed below, carbon bonded into the Si-O-C network could be also responsible for a part of the absorption in the regions of Si-O-Si vibrations.

The broad peak ranging from 3000 to 3700 cm^{-1} was related to the presence of OH groups. It was composed of two peaks centered at about 3400 and 3650 cm^{-1} that can be associated with the stretching of hydrogen-bonded and free O-H groups, respectively. Further evidence of OH groups comes from the peak at 930 cm^{-1} assigned to Si-OH stretching. These absorption peaks were detected at both pressures.

Besides the peaks mentioned above, the IR spectra of the film deposited at 2.5 Pa comprised a narrow strong peak at 2340 cm^{-1} and two weak peaks at 1620 and 1715 cm^{-1}. Asymmetric stretching of gaseous CO_2 appears as two peaks at 2360 and 2337 cm^{-1} due to its rotation **?**. Since the infrared spectrometer was evacuated down to 2.5 hPa for the measurement the background atmosphere was very reproducible and no such uncompensated CO_2 peaks originating from the background gas were ever observed. Therefore the peak at 2340 cm^{-1} was assigned to CO_2 trapped in the film structure. The confinement of CO_2 restricted its rotational motion and led to distortion of the rotational band structure observed as an increase and narrowing of the peak at 2340 cm^{-1} and diminishing of the peak at 2360 cm^{-1}. Similar peak was also observed by Theil *et al.*and interpreted as a postdeposition reaction of CO_2 with nanoporous films Theil et al. (1994). In our case it appeared only for low pressure deposition during which dc self-bias voltage was -110 V, i. e., much higher than -20 V at the pressure of

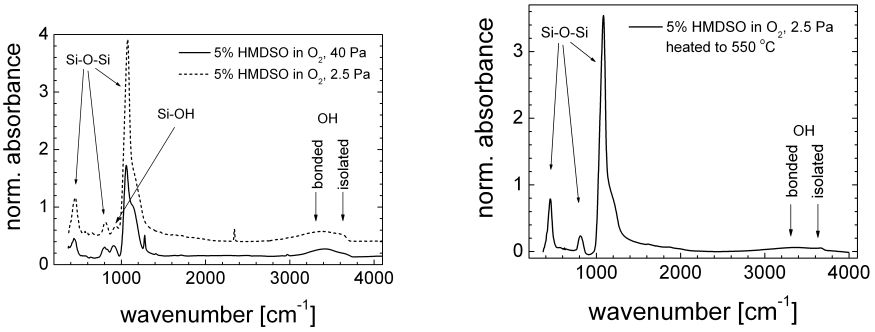

Fig. 1. IR absorbances divided by the film thickness for the films deposited from 5 % HMDSO in oxygen at two different pressures, 2.5 and 40 Pa and correspondingly different dc self-bias -110 and -20 V (left). Normalized IR absorbance for the film deposited at 2.5 Pa and subsequently heated to 500 °C in vacuum (right).

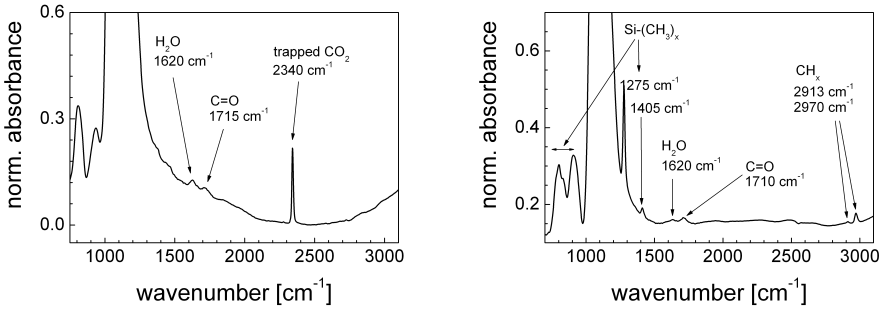

Fig. 2. Details of normalized absorbances for the films deposited from 5 % HMDSO in oxygen at 2.5 Pa (left) and 40 Pa (right)

40 Pa. As mentioned above, the energy of the ions accelerated in the plasma sheath towards the growing film was much lower at the pressure of 40 Pa due to lower self-bias and higher probability of ion collisions. Therefore, it was concluded that CO_2^+ ions were implanted into the film structure in case of the deposition at 2.5 Pa. It can correspond also to the presence of the weak peak at 1715 cm^{-1} assigned to carbonyl stretching Theil et al. (1994); Fleyfel & Devlin (1991). The second weak peak found at 1620 cm^{-1} was associated with trapped water molecules **?**.

The IR spectra of the films deposited at 40 Pa were more complicated due to higher amount of carbon-related groups. The peak at about 800 cm^{-1} was obviously composed of at least three peaks centered at about 780, 800 and 840 cm^{-1} corresponding to CH_3 rocking or Si-C stretching in Si-$(CH_3)_x$ groups ($x = 1 \ldots 3$) Kashiwagi et al. (1991); **?**); Lamendola et al. (1997). The peak at 905 cm^{-1} is probably composed of two peaks, the peak corresponding to Si-OH stretching observed at 930 cm^{-1} for the low pressure deposition and the peak at 890 cm^{-1} assigned to CH_3 rocking or Si-C stretching in Si-$(CH_3)_2$. The summary of Si-$(CH_3)_x$ related peaks that can be, according to the literature, found in the region 760–890 cm^{-1} is given in Ta-

σ (cm^{-1})	Mode	Comment	Ref.
CH_x correlated peaks			
2960	$\nu^{a}_{CH_3}$		Smith (1977); Dischler et al. (1983)
2900	$\nu^{s}_{CH_3}$		Smith (1977); Dischler et al. (1983)
2925	$\nu^{a}_{CH_2}$		Smith (1977); Dischler et al. (1983)
2855	$\nu^{s}_{CH_2}$		Smith (1977); Dischler et al. (1983)
1460	$\delta^{a}_{CH_2}$		Smith (1977); Dischler et al. (1983)
$Si-CH_2$ correlated peaks			
1360	δ_{CH_2}	in Si-CH_2-Si	Anderson (1974)
1400	δ_{CH_2}	in Si-$(CH_2)_2$-Si	Anderson (1974)
$Si-CH_3$ correlated peaks			
1410	$\delta^{a}_{CH_3}$	in Si-Me_x	Anderson (1974)
1260	$\delta^{s}_{CH_3}$	in Si-Me_x	Anderson (1974)
845	ρ_{CH_3}, ν_{SiC}	in Si-Me_3	Anderson (1974)
760	ρ_{CH_3}, ν_{SiC}	in Si-Me_3	Anderson (1974)
885	ρ_{CH_3}, ν_{SiC}	in Si-Me_2	Anderson (1974)
805	ρ_{CH_3}, ν_{SiC}	in Si-Me_2	Anderson (1974)
775	ρ_{CH_3}, ν_{SiC}	in Si-Me_1	Anderson (1974)
$Si-H$ correlated peaks			
2140	ν_{SiH}		Anderson (1974)

Table 1. Assignment of FTIR peaks observed in the deposited films. Greek letters ν, δ and ρ denote stretching, bending and rocking modes, respectively.

ble 1. Further evidence of Si-(CH_3) groups is revealed by the strong narrow peak at 1275 cm^{-1} and weak peak at 1405 cm^{-1} associated with symmetric and asymmetric bending of methylsilyl groups, respectively **?**.
2913, 2970
It can be seen from IR spectra that even though the concentration of HMDSO in O_2 was as low as 5 % the HMDSO was not fully oxidized in the deposit. Quantitative results on atomic concentration of impurities were obtained by the combination of RBS and ERDA measuremets (Table 3). The film deposited at the pressure of 40 Pa contained 10 % of carbon whereas the atomic percentage of carbon in the film deposited at 2.5 Pa was 1 % only that corresponded with the IR spectra showing much higher peak of Si-CH. The original monomer was indeed more oxidized in case of lower pressure because oxygen-to-silicon ratio was 2.46 and 1.75 for 40 and 2.5 Pa, respectively. Part of oxygen atoms was, however, not fully bonded in the cross-linked Si-O-Si network but terminated by hydrogen. The hydrogen content was quite similar, 22 and 20 %, for both the pressures. High amount of OH groups was indeed revealed by the absorption peaks in FTIR measurements whereas SiH groups were not detected (Figs. **??** and **??**).
Different chemical structure and composition was also reflected in very different functional properties of these two films. The low pressure film had the indentation hardness of 6.9 GPa and was almost stress free. The high pressure film was quite soft having the indentation hardness of 1.6 GPa only and exhibited high tensile intrinsic stress. DODELAT
The film deposited at 2.5 Pa, exhibiting quite good mechanical properties, was tested for thermal stability by its heating to 500 °C in vacuum. This treatment was monitored by in-situ mass spectrometry of desorbing species Zajíčková, Buršíková, Kučerová, Franclová, Šťahel,

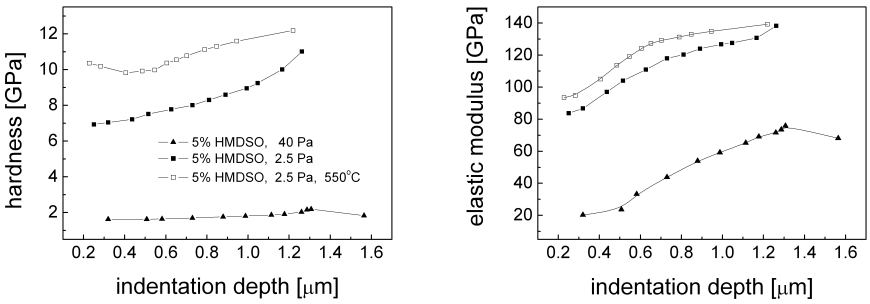

Fig. 3. Indentation hardness and elastic modulus in dependence on indentation depth for the films deposited from 5 % HMDSO in oxygen on silicon substrates. The measurements were carried out on as-deposited films and the film heated in vacuum to 500 °C.

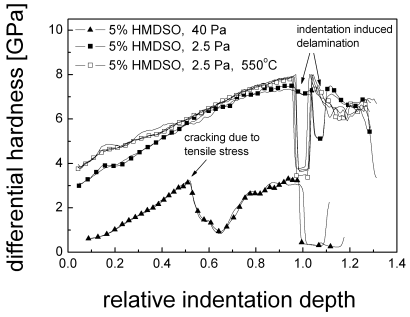

Fig. 4. Differential hardness in dependence on relative indentation depth, i. e., depth divided by film thickness, for the films deposited from 5 % HMDSO in oxygen on silicon substrates. The measurements were carried out on as-deposited films and the film heated in vacuum to 500 °C.

Peřina & Macková (2007). The desorption of water reached its maximum at 210 °C. Further desorbing species had two maxima, the first at the same temperature and the second between 375–440 °C. Their identification was complicated by dissociation in the mass spectrometer. It was obvious that CO_2 was released by heating and it confirmed its presence discovered by FTIR analysis. The signal of CO could be composed from desorbing molecules as well as dissociation of CO_2. Additionally, the CH_x species were detected too. The infrared spectrum of the heated film exposed to atmosphere are shown in Fig. 1. The peaks corresponding to CO_2 and Si-OH completely disappeared and the peaks related to bonded and isolated OH groups were significantly reduced.

The changes of chemical structure with heating caused also increased hardness and elastic modulus as can be seen from Figs. **??** and **??**. DODELAT

mixture	p [Pa]	P [W]	U_b [V]	H_{IT} [GPa]	E_{IT} [GPa]	Si [%]	O [%]	C [%]	H [%]
5 % HMDSO/O_2	40	100	-20	1.6 ± 0.3	8 ± 1	25	43	10	22
5 % HMDSO/O_2	2.5	100	-110	6.9 ± 0.5	63 ± 4	23	56	1	20
8 % HMDSO/O_2	27	100	-50	2.4 ± 0.2	24 ± 2	21	40	14	26
8 % HMDSO/O_2	27	450	-100	5.7 ± 0.3	57 ± 3	22	47	5	25
17 % HMDSO/O_2	4	100	-110	1.7 ± 0.1	19 ± 2	16	32	14	38
17 % HMDSO/O_2	4	450	-250	9.9 ± 0.3	75 ± 3	20	37	11	32
100 % HMDSO	1	100	-140	0.3 ± 0.1	5 ± 1	16	12	19	53
100 % HMDSO	1	450	-335	11.2 ± 0.3	73 ± 3	21	11	30	39

Table 2. Summary of deposition conditions (pressure - p, rf power P and dc self-bias U_b, mechanical properties determined by depth-sensing indentation of the films deposited on Si (indentation hardness - H_{IT} and modulus - E_{IT}) and atomic composition determined by combination of RBS and ERDA. The results are shown for as-deposited films.

mixture	p [Pa]	P [W]	T [°C]	H_{IT} [GPa]	E_{IT} [GPa]	Si [%]	O [%]	C [%]	H [%]
5 % HMDSO/O_2	2.5	100	500			–	–	–	–
8 % HMDSO/O_2	27	100	300			22	37	13	29
8 % HMDSO/O_2	27	100	500			22	40	11	28
8 % HMDSO/O_2	27	450	300	7.3 ± 0.7	64 ± 3	25	48	7	20
8 % HMDSO/O_2	27	450	500	11.3 ± 0.5	75 ± 2	27	52	6	15
17 % HMDSO/O_2	4	100	300			19	31	15	35
17 % HMDSO/O_2	4	100	500			20	35	13	32
17 % HMDSO/O_2	4	450	300	10.7 ± 0.5	73 ± 5	21	38	12	29
17 % HMDSO/O_2	4	450	500	11.4 ± 0.5	81 ± 3	22	44	12	22

Table 3. Mechanical properties and atomic composition of the films from Table 3 heated in vacuum to temperature T.

7. Deposition from 8 % HMDSO/O_2 gas feed at pressure of 27 Pa

The deposition from 8 % HMDSO/O_2 at pressure of 27 Pa was tested for different rf power, 100 and 450 W, that corresponded to the dc self-bias of -50 and -100 V. The residence time was similar to the 5 % HMDSO/O_2 deposition at pressure of 40 Pa (section 6) but the energy of bombarding ions was slightly higher. The normalized absorbances are given in Fig. 5. The typical structure of SiO_2 absorption and the presence of OH groups can be seen again in the overview spectra (left). Zooming into the details (right) shows the presence of other chemical groups related to carbon and hydrogen impurities.

Comparison of the IR absorbances for the films deposited from 5% and 8% mixtures (Figs. 2 and 5) at 100 W and higher pressure, 40 and 27 Pa, respectively, reveals their similar chemical structure. Both the films contain methylsilyl groups evidenced by the overlapped peaks in the region 760–890 cm^{-1}, strong narrow peak at 1275 cm^{-1} and weak peak at 1410 cm^{-1}. The presence of CH_x groups caused also the absorption peaks in the region 2910–2970 cm^{-1}.

The film deposited at higher power 450 W and correspondingly higher dc self-bias contained much less CH_x groups because of higher ion energy leading to more cross-linked film. The peaks in the range 2910–2970 cm^{-1} and the peak at 1405 cm^{-1} were hardly visible. The peak

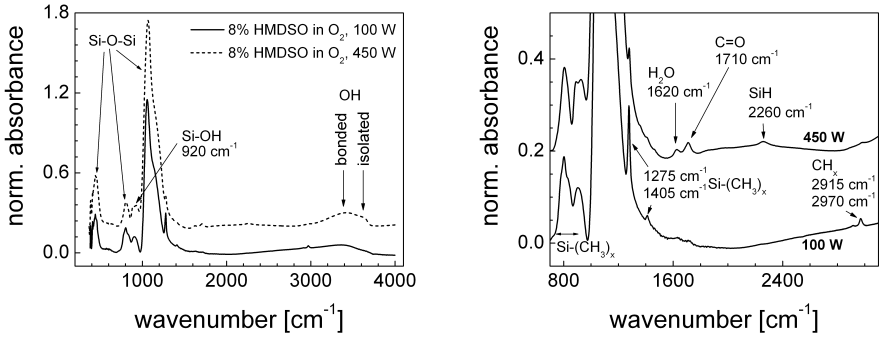

Fig. 5. Normalized absorbances for the films deposited from 8 % HMDSO in oxygen at 27 Pa and different rf power.

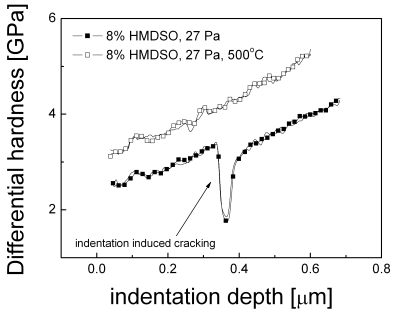

Fig. 6. Differential hardness in dependence on relative indentation depth, i. e., depth divided by film thickness, for the films deposited from 8 % HMDSO in oxygen on silicon substrates. The measurements were carried out on as-deposited films and the film heated in vacuum to 500 °C.

at 1275 cm^{-1} was quite weak, the peak at 806 cm^{-1} was narrower, i. e., Si-O-Si bending was not overlapped with the Si-$(CH_3)_x$ peaks of similar intensity, and the absorption at about 910 cm^{-1} was clearly splitted between the peak corresponding to rocking or stretching in Si-$(CH_3)_2$ at 890 cm^{-1} and stretching in Si-OH at 930 cm^{-1}. The spectra shows also the presence of trapped water and C=O. The new weak peak that appeared at 2260 cm^{-1} corresponded to Si-H stretching.

The optical properties in UV/VIS range of both the films were close to the fused silica. The refractive index at 600 nm was 1.44 and 1.47 for 100 and 450 W, respectively, and the extinction coefficient at 240 nm was below 0.003. The films exhibited a small compressive stress, especially for higher power. The more cross-linked film prepared at 450 W had significantly higher plastic hardness and elastic modulus (Table 3).

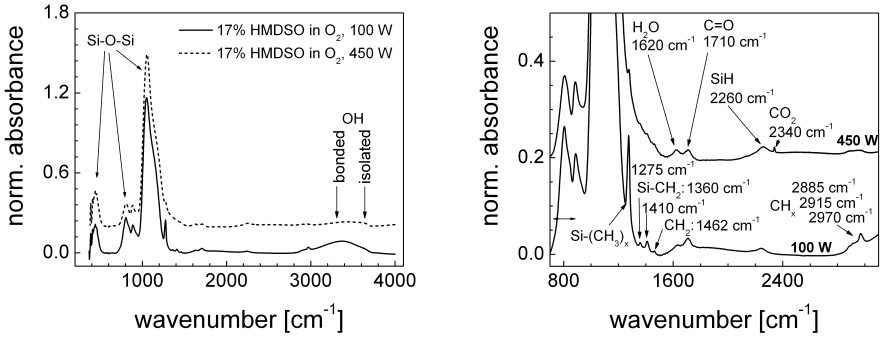

Fig. 7. Normalized absorbances for the films deposited from 17 % HMDSO in oxygen at 4 Pa and different rf power.

8. Deposition from 17 % HMDSO/O_2 gas feed at pressure of 4 Pa

Due to decreased flow rate of oxygen and non-linear pumping speed for different flow rates the pressure of the deposition was significantly lower for 17 % HMDSO/O_2 mixture. It resulted in higher dc bias, i. e., -110 and -250 V, corresponding to 100 and 450 W, respectively, and shorter residence time of 4 s. Notice that from this respect the deposition at 100 W was similar to the deposition at 2.5 Pa and 5 % HMDSO/O_2.

9. Deposition from 29 % HMDSO/O_2 gas feed at pressure of 2.5 Pa

10. Deposition from 44 % HMDSO/O_2 gas feed at pressure of 2 Pa

11. Deposition from pure HMDSO gas feed

Films from pure HMDSO were prepared at four different powers, 100, 200, 300 and 450 W. The corresponding dc self-biases were -145, -215, -270 and -335 V, respectively. The collisions in the sheath can be neglected at the deposition pressure, 1 Pa, and therefore, the energy of ions approached the self-bias. The modification of the film chemical structure deposited at 450 W by increased ion energy was significant as seen from the comparison of FTIR spectra in Fig. 8. The film deposited at low powers contained Si-O-Si groups evidenced by a small peak at 430 cm^{-1} and higher intensity of the strong peak at 1035 cm^{-1}. The latter can be, however, caused also by the presence of Si-O-C groups.

The CH stretching band of the film deposited at 100 W was dominated by the peak at 2965 cm^{-1} assigned to sp^3C-H_3 asymmetric stretching. A related symmetric stretching peak at 2870 cm^{-1} was strongly overlapped by surrounding peaks at 2860 cm^{-1}(sp^3C-H_2 sym.) and 2910 cm^{-1} (sp^3C-H). A rearrangement of CH_x groups even at the lowest annealing temperature of 300 °C can be seen in Fig. **??**. The peaks corresponding to asym. and sym. stretching of sp^3C-H_2 (2930 and 2860 cm^{-1}) became clearly visible after the annealing. At 500 °C the peaks of sp^3C-H_2 increased obviously on the expenses of sp^3C-H_3. A significant decrease of C-H_3 groups bonded to Si is demonstrated by a decrease of the peak at 1265 cm^{-1}.

The double peak positioned at 2160 and 2220 cm^{-1} decreased with annealing temperature. In this region the absorption can be caused either Si-H or C≡N bonds. Nitrogen could be

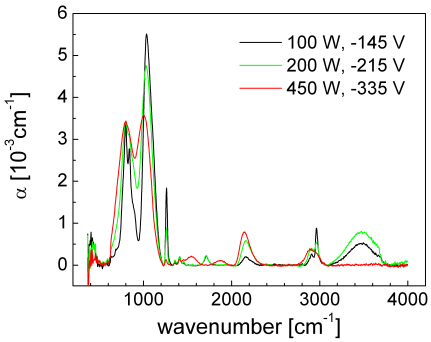

Fig. 8. Normalized absorbances for the films deposited from 100 % HMDSO at 1 Pa and different rf powers.

present only as small impurity and also based on the annealing experiment the Si-H is the most probable. Two positions can be explained by different surrounding of these groups.
The restructuring caused slightly higher hardness of the films that increased from 1.8 to 3.3 GPa.

12. References

Alt, L. L., Ing, Jr., S. W. & Laendle, K. W. (1963). Low-temperature deposition of silicon oxide films, *J. Electrochem. Soc.* **110**: 465.

Anderson, D. R. (1974). *Analysis of Silicones*, Wiley-Interscience, New York, chapter Infrared, Raman and Ultraviolet Spectroscopy.

Angelini, E., d'Agostino, R., Fracassi, F., Grassini, S. & Rosalbino, F. (2002). Surface analysis of PECVD organosilicon films for corrosion protection of steel substrates, *Surf. Interface Anal.* **34**: 155–159.

Bauser, H., Benz, V., Heinemann, M. & Schindler, B. (1994). Verfahren zum Erzeugen von siliciumoxidischen kratzfesten Schichten auf Kunststoffen durch Plasmabeschichtung. European Patent 590 467 A1.

Benz, G., Mutshler, G. & Schneider, G. (1985). Verfahren zum Aufbringen einer dünnen, transparenten Schicht auf der Oberfläche optischer Elemente. Germany Patent DE 3413019.

Borvon, G., Goullet, A., Granier, A. & Turban, G. (2002). Analysis of low-k organosilicon and low-density silica films deposited in HMDSO plasmas, *Plasmas and Polymers* **7**(4): 341–352.

Borvon, G., Goullet, A., Mellhaoui, X., Charrouf, N. & Granier, A. (2003). Electrical properties of low-dielectric-constant films prepared by PECVD in O_2/CH_4/HMDSO, *Materials Science in Semiconductor Processing* **5**: 279–284.

Chin, B. L. & de Ven, E. P. V. (1988). Plasma TEOS process for interlayer dielectric applications, *Solid State Technol.* **13**: 119–122.

D. Korzec, K. Traub, F. W. & Engemann, J. (1996). Remote deposition of scratch resistant films by use of slot antenna microwave plasma source, *Thin Solid Films* **281-282**: 143–145.

Dischler, B., Bubenzer, A. & Koidl, P. (1983). Bonding in hydrogenated-hard carbon studied by optical spectroscopy, *Solid State Communications* **48**(2): 105–108.

Ebihara, K., Fujishima, T., Kojyo, D. & Murata, M. (1993). Silicon oxide film preparation by rf plasma-enhanced MOCVD using hexamethyldisiloxane, *Plasma Sources Sci. Technol.* **2**: 14–17.

Fleyfel, F. & Devlin, J. P. (1991). Carbon-dioxide clathrate hydrate epitaxial-growth-spectroscopic evidence for formation of the simple type-ii co2 hydrate, *J. Phys. Chem.* **95**: 3811–3815.

Fujino, K., Nishimoto, Y., Tokumasu, N. & Maeda, K. (1992). Low temperature, atmospheric pressure CVD using hexamethyldisiloxan and ozone, *J. Electrochem. Soc.* **139**(8): 2282–2287.

Hollahan, J. R. & T. Wydeven, J. (1977). Verfahren zum Beschichten von Kunststoffgegenständen und -flächen. Germany Patent DE 2650048 C2.

Ing, S. W. & Jr., W. D. (1965). Glow discharge formation of silicon oxide and the deposition of silicon oxide thin film capacitors by glow discharge techniques, *J. Electrochem. Soc.* **112**: 284.

Kageyama, Y. & Taga, Y. (1987). The surface hardening of transparent plastics by PVD method, *Proceedings of ISPC-8, Tokyo*, pp. 1073–1078.

Kashiwagi, K., Yoshida, Y. & Murayama, Y. (1991). Hybrid films formed from hexamethyldisiloxane and sio by plasma process, *Jap. J. Appl. Phys.* **30**(8): 1803–1807.

Kulisch, W., Lippmann, T. & Kassing, R. (1989). Plasma-enhanced chemical vapour deposition of silicon dioxide using tetraethoxysilane as silicon source, *Thin Solid Films* **174**: 57.

Lamendola, R., D'Agostino, R. & Fracasi, F. (1997). Thin film deposition from hexamethyldisiloxane fed glow discharges, *Plasmas and Polymers* **2**(3): 147–164.

Levy, R. A., Ramos, E. S., Krasnoperov, L. N., Datta, A. & Grow, J. M. (1996). Microporous SiO_2/Vycor membranes for gas separation, *J. Mater. Res.* **11**(12): 3164–3173.

Pai, C. S. & Chang, C.-P. (1990). Downstream microwave plasma-enhanced chemical vapor deposition of oxide using tetraethoxysilane, *J. Appl. Phys.* **68**(2): 793–801.

Ray, S. K., Maiti, C. K., Lahiri, S. K. & Chakrabarti, N. B. (1992). Properties of silicon dioxide films deposited at low temperatures by microwave plasma enhanced decomposition of tetraethylorthosilicate, *J. Vac. Sci. Technol. B* **10**(3): 1139–1150.

Reed, C. W., Rzad, S. J. & Devins, J. C. (1989). Abrasion-resistant plastic articles and method for making them. WO Patent 89/01957.

Reed, C. W., Rzad, S. J. & Devins, J. C. (1991). Abrasion-resistant plastic articles. US Patent 5,569,497.

Rossnagel, S. M., Cuomo, J. J. & Westwood, W. D. (eds) (1989). *Handbook of plasma processing technology (Fundametals, Etching, Deposition, and Surface Interaction)*, Noyes Publications, New Jersey.

Schreiber, H. P., Wertheimer, M. R. & Wrobel, A. M. (1980). Corrosion protection by plasma-polymerized coatings, *Thin Solid Films* **72**: 487–493.

Secrist, D. R. & Mackenzie, J. D. (1966). Deposition of silica films by the glow discharge techniques, *J. Electrochem. Soc.* **113**: 914.

Selamoglu, N., Mucha, J. A., Ibbotson, D. E. & Flamm, D. L. (1989). Silicon oxide deposition from tetraethoxysilane in a radio frequency downstream reactor: Mechanismus and step coverage, *J. Vac. Sci. Technol. B* **7**(6): 1345–1351.

Smith, A. L. (1977). *Applied Infrared Spectroscopy*, Wiley, New York, p. 286.

Theil, J. A., Brace, J. G. & Knoll, R. W. (1994). Carbon content of silicon oxide films deposited by room temperature plasma enhanced chemical vapor deposition of hexamethyldisiloxane and oxygen, *J. Vac. Sci Technol. A* **12**(4): 1365–1370.

Tien, P. K., Smolinsky, G. & Martin, R. J. (1972). Thin organosilicon films for integrated optics, *Applied Optics* **11**(3): 637–642.

Vallée, C., Goullet, A., Granier, A., Lee, A. v. d., Durand, J. & Marlière, C. (2000). Inorganic to organic crossover in thin films deposited from O_2/TEOS plasmas, *J. Non-Cryst. Solids* **272**: 163–173.

Vasile, M. J. & Smolinski, G. (1972). Organosilicon films formed by an r.f. plasma polymerization process, *J. Electrochem. Soc.* **119**(4): 451–455.

Williams, J. L., Burkett, S. L. & McGuire, S. (1994). Process for barrier coatings of plastic objects. US Patent 5,364,666.

Wrobel, A. M. & Wertheimer, M. R. (1990). Plasma-polymerized organosilicones and organometallics, *in* R. d'Agostino (ed.), *Plasma Deposition, Treatment and Etching of Polymers*, Academic Press, New York, pp. 163–268.

Wydeven, T. (1977). Plasma polymerized coating for polycarbonate: single layer, abrasion resistant, and antireflection, *Appl. Optics* **16**(3): 717–721.

Zajíčková, L., Buršíková, V., Franta, D., Bousquet, A., Granier, A., Goullet, A. & Buršík, J. (2007). Comparative study of films deposited from HMDSO/O_2 in continuous wave and pulsed rf discharges, *Plasma Processes and Polymers* **4**: S287–S293.

Zajíčková, L., Buršíková, V. & Janča, J. (1998). Protection coatings for polycarbonates based on PECVD from organosilicon feeds, *Vacuum* **50**(1-2): 19–21.

Zajíčková, L., Buršíková, V., Kučerová, Z., Franclová, J., Šťahel, P., Peřina, V. & Macková, A. (2007). Organosilicon thin films deposited by plasma enhanced cvd: Thermal changes of chemical structure and mechanical properties, *J. Phys. Chem. Solids* **68**: 1255–1259.

Zajíčková, L., Buršíková, V., Kučerová, Z., Franta, D., Dvořák, P., Šmíd, R., Peřina, V. & Macková, A. (2007). Deposition of protective coatings in rf organosilicon discharges, *Plasma Sources Sci. Technol.* **68**(1): S123–S132.

Zajíčková, L., Buršíková, V., Peřina, V., Macková, A., Subedi, D., Janča, J. & Smirnov, S. (2001). Plasma modification of polycarbonates, *Surf. Coat. Technol.* **142-144**: 449–454.